NANO LETTERS

Letter

pubs.acs.org/NanoLett

Aluminum Plasmonic Multicolor Meta-Hologram

Yao-Wei Huang,[†] Wei Ting Chen,[†] Wei-Yi Tsai,[†] Pin Chieh Wu,[†] Chih-Ming Wang,[‡] Greg Sun,[§] and Din Ping Tsai*[,†,∥]

[†]Department of Physics, National Taiwan University, Taipei 10617, Taiwan

[‡]Institute of Opto-electronic Engineering, National Dong Hwa University, Hualien 97401, Taiwan

[§]Department of Engineering, University of Massachusetts Boston, Boston, Massachusetts 02125, United States

[∥]Research Center for Applied Sciences, Academia Sinica, Taipei 11529, Taiwan

Supporting Information

ABSTRACT: We report a phase-modulated multicolor meta-hologram (MCMH) that is polarization-dependent and capable of producing images in three primary colors. The MCMH structure is made of aluminum nanorods that are arranged in a two-dimensional array of pixels with surface plasmon resonances in red, green, and blue. The aluminum nanorod array is patterned on a 30 nm thick SiO_2 spacer layer sputtered on top of a 130 nm thick aluminum mirror. With proper design of the structure, we obtain resonances of narrow bandwidths to allow for implementation of the multicolor scheme. Taking into account of the wavelength dependence of the diffraction angle, we can project images to specific locations with predetermined size and order. With tuning of aluminum nanorod size, we demonstrate that the image color can be continuously varied across the visible spectrum.

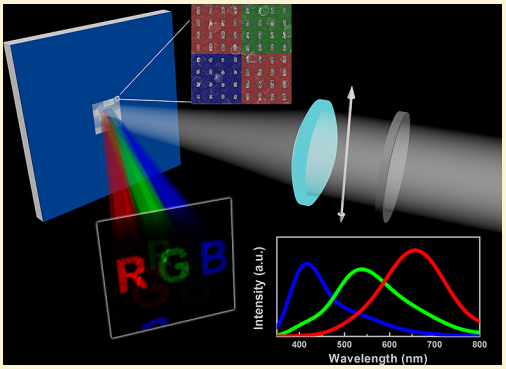

KEYWORDS: *Metasurfaces, aluminum plasmonics, meta-hologram, holography, nanoantennas, multicolor, polarization, switching*

Sense of color by human beings is through the photoreceptors on retinas called cones and visual pigments that are particularly sensitive to blue, green, and red light.[1,2] Nowadays, vision technologies in various color applications are primarily targeting these three colors and their mixing in conjunction with control of light polarization. The demonstration of white light viewable hologram known as the rainbow hologram has transformed the display holography, and the multicolor holograms were quickly sought after for artistic and commercial displays. However, its adoption has been limited by a rather serious deficiency that the colors of the reconstructed image tend to vary from different viewing angles, implying that real colors of the reconstructed image are not properly preserved. Traditional full-color holograms, like the 3D full-color Denisyuk hologram, use transparent films fabricated with three primary color photoresists.[3] Spatial light modulators (SLM) that dynamically modulate a beam of light by altering the phase and amplitude have been respectively applied in liquid crystal displays (LCD)[4] and in digital micromirror devices (DMD).[5] However, the scalar diffractive pattern employed in these techniques renders polarization unswitchable, and the photoresists are always rather thick compared to the wavelength of light. Recent development in hologram employs vector diffractive optics that promises maximal storage of information over minimal storage area. Using amplitude modulation, Osaki et al. demonstrated the multiplexed thin hologram based on different gratings for light of three primary colors on a silver film deposited on a glass prism, radiating surface plasmons into free space.[6] In the past decade, metamaterials/metasurfaces composed of subwavelength artificial structures show tailored optical properties, enabling holograms in a wide range of electromagnetic region.[7−11] Metamaterials with tunable effective refractive indices by design have been applied to holograms in which switchable polarizations and dual images of different wavelengths were demonstrated in the near-IR region.[12,13] Montelongo et al. demonstrated a two-color (blue and red) amplitude-modulated hologram based on plasmonic silver nanoparticle scattering.[14,15] These results suggest that metasurfaces are better employed to obtain SLM, and they have been explored to realize polarization-controlled dual images at desirable spectral regions referred to as multiband metasurface hologram or meta-hologram.[16−20] Between the two modulation approaches commonly employed in holography, the spatial phase modulation is more desirable than that of amplitude because the former typically yields brighter image by preserving its reflectance. Unfortunately, metasurface-based full or multicolor holograms demonstrated so far employed mostly amplitude modulation because efficient phase modulation covering the entire visible spectrum is difficult if not impossible to realize for gold and silver when their feature dimensions are about few tens of nanometers; e.g., phase modulation with gold does not

Received: January 16, 2015
Revised: April 3, 2015
Published: April 6, 2015

DOI: 10.1021/acs.nanolett.5b00184
Nano Lett. 2015, 15, 3122−3127

work for wavelengths below 650 nm[18] while that of silver does not have access to the blue region (see Supporting Information part 1). In addition, color multiplexing has been extremely difficult to achieve in broadband meta-hologram.[17−20] Interestingly, aluminum with higher plasma frequency[21] has recently been studied to yield surface plasmon resonances across a broader range of the spectrum spanning from visible to UV;[22,23] such advances have led to demonstration of vivid color plasmonic pixels,[24] plasmonic color printing,[25,26] and plasmonic spectral color filters.[27,28] Metasurfaces incorporating aluminum offer the unique opportunity to extend the working wavelength to cover the entire visible spectrum for the generation of full-color meta-holograms.

Here we present a phase modulated multicolor meta-hologram (MCMH) based on an optically thin reflective metasurface that enables formation of polarization-dependent images in three primary colors. Figure 1a shows the schematic setup of MCMH under *y*-polarized white light illumination (consisting of 405, 532, and 658 nm laser beams) that reconstructs images "R" in red, "G" in green, and "B" in blue, respectively. The MCMH consists of 180 × 180 pixels, each made of 4 subpixels; one for blue, one for green, and two for red to compensate for the lower reflectance in red. The metasurfaces with patterned nanorod array in each pixel yield the required phase distribution of a computer-generated hologram (CGH) designed by iterative Fourier-transform algorithm (IFTA).[29] Each subpixel has 4 × 4 aluminum nanorods patterned on top of a 30 nm thick SiO_2 spacer layer sputtered on a 130 nm thick aluminum mirror. To simplify the fabrication process, all nanorods are designed to have the same width of 50 nm and same thickness of 25 nm with only their lengths varied to generate the required phase and reflectance (inset in Figure 2a). The three ideal images designed in three primary colors (red R, green G, and blue B) are shown in Figure 1b. To compensate for the chromatic dispersion of the reconstructed image caused from the wavelength dependence of the diffraction angle, we have normalized the sizes of the letters in order for the images to appear in the right spatial order with equal size.

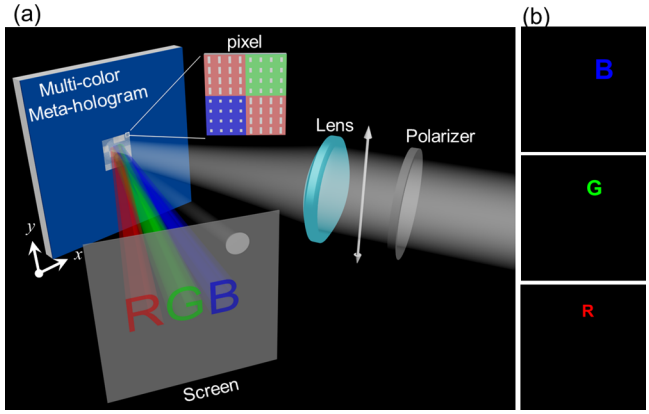

Figure 1. (a) Illustration of the designed multicolor meta-hologram (MCMH) under linearly polarized illumination. The MCMH structure is made of a pixel array consisting of aluminum nanorods that produce images R, G, and B in 405, 532, and 658 nm, respectively. The pixels are patterned on a 30 nm thick SiO_2 spacer sputtered on an aluminum mirror. (b) The sizes and locations of the three images R, G, and B relative to the zeroth-order spot located at the upper right corner of the image screen that are designed to make the reconstructed images fall into the right spatial order with the appearance of equal size.

Design and Fabrication of MCMH. Using the finite-difference time-domain (FDTD) method (CST Microwave Studio), we have simulated the reflectance and phase modulation of the periodically patterned aluminum nanorods under the normal illumination of *y*-polarized light. A unit cell with its dimensions is shown in the inset of Figure 2a. Figures 2a and 2b show the reflective spectra and phase as a function of rod length. The resonance shifts from 375 to 800 nm with the increase of rod length from 50 to 150 nm, spanning the entire visible spectrum. A similar structure made of gold-nanorods/MgF_2/gold-mirror capable of obtaining large phase modulation of the reflection has been previously applied to broadband phase hologram with conserved linear polarization[10,18] and anomalous circularly polarized waves[20] but failed to yield color multiplexing in the visible spectrum. Here we use the aluminum-nanorods/SiO_2/aluminum-mirror structure to expand the resonance spectral range all the way down to 375 nm, allowing for meta-holograms capable of generating images of any color in the visible spectrum. Figure 2c shows the dependence of reflectance and phase modulation on the nanorod length for the three primary colors at λ = 405, 532, and 658 nm. Two of the challenges for the multicolor operation of a meta-hologram are efficiency and crosstalk. Narrow resonances of the nanorods are generally favorable for minimizing the crosstalk between different color images, but this also implies that the usable range of the incident wavelength range is reduced, resulting in lower efficiencies of the reconstructed images. Our design of the MCMH takes both into consideration with the two-level phase modulation scheme. Such a scheme requires only two different lengths of nanorods for each color with two different resonances. For the three color demonstration, we have six resonances in the visible range. In comparison with other schemes of higher phase levels, e.g., a four-level phase modulation would result in 12 resonances in the visible range, the two-level design employed in the MCMH is not only easier to fabrication but far more effective in minimizing crosstalk. The two different rod lengths were chosen for each wavelength (color) in such a way that they yield a phase difference of π while maintaining approximately the same reflectance. The structure of MCMH consists of many pixels. Each pixel in turn has four subpixels made of 4 × 4 aluminum nanorods. Among them, one for blue, one for green, and two for red. Within each subpixel, all nanorods have the same dimensions, but subpixels from different pixels can have different dimensions to yield either 0 or π phase for a given color. The arrangement of a particular size of the nanorods in a subpixel located inside of a pixel is determined by the phase requirement obtained by the iterative Fourier-transform algorithm (IFTA) of the image letters (Figure 1b) to be reconstructed. As such, six different kinds of subpixels are necessary corresponding to two phase levels at three operating wavelengths. The blue circles, green triangles, and red squares shown in Figures 2a−c indicate the rod lengths of 55, 70, 84, 104, 113, and 128 nm with their corresponding reflectance and phase modulations we have selected to realize the MCMH.

The MCMH was fabricated with standard e-beam lithography (see Supporting Information part 2). Figure 2d shows the scanning electron microscope (SEM) image of a small region of the fabricated sample. The corresponding rod lengths for the binary phases are used to form the subpixels; each of them occupies an area of 800 × 800 nm^2 consisting of 4 × 4

DOI: 10.1021/acs.nanolett.5b00184
Nano Lett. 2015, 15, 3122−3127

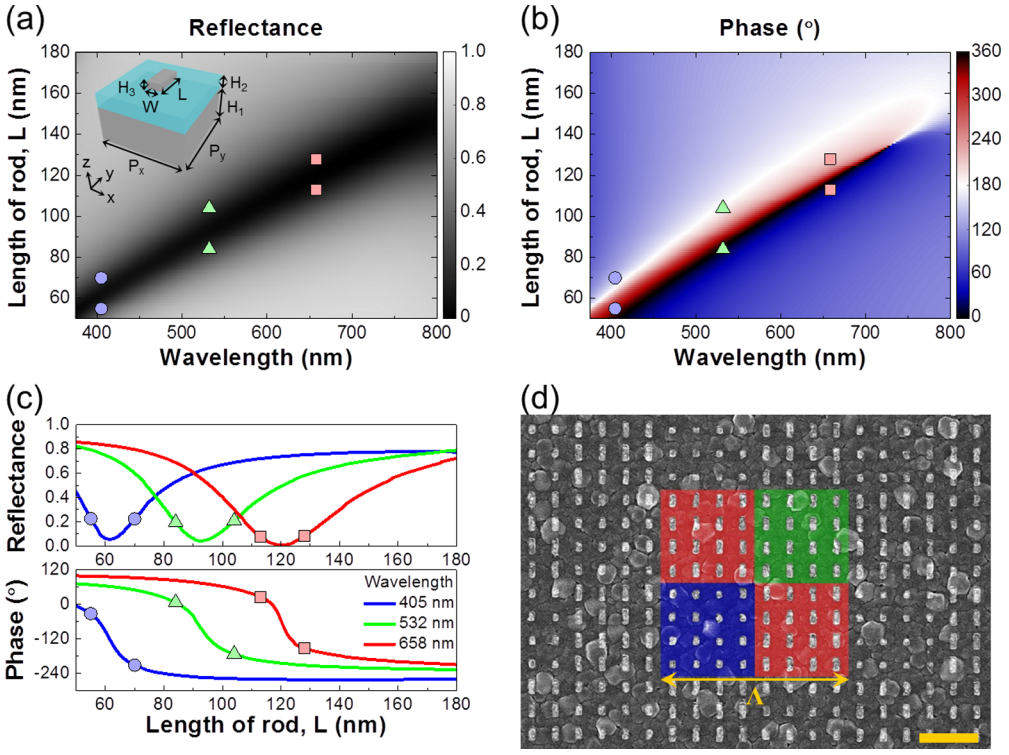

Figure 2. Simulated (a) reflectance and (b) phase distribution as a function of wavelength and length of the aluminum nanorod (inset). Unit cell dimensions: periodicity $P_x = P_y = 200$ nm, thickness of aluminum mirror $H_1 = 130$ nm, thickness of SiO_2 $H_2 = 30$ nm, thickness of nanrod $H_3 = 25$ nm, and width of nanorod $W = 50$ nm. (c) Simulated reflectance vs nanorod length and its phase for wavelengths 405, 532, and 658 nm. The two blue circles in (a–c) indicate two nanorod lengths that produce the phase separation of π, which we have chosen to construct the blue part of the MCMH. Similarly, the two green triangles and the two red squares are for the green and red part of the pixels, respectively. (d) SEM image of the MCMH sample. The colored area forms a pixel with four subpixels. The scale bar is 500 nm, and the size of each pixel Λ is 1600 nm.

aluminum nanorods of equal dimensions. Four such subpixels (two for red, one for green, and one for blue) make up a pixel. Based on our simulation, the reflectance for $\lambda = 405$, 532, and 658 nm are 22%, 19%, and 7.3%, respectively, which is the reason for using two subpixels for red to compensate for its low reflectance. The MCMH sample was fabricated on a total area of 288 × 288 μm^2 consisting of 180 × 180 pixels.

Reconstructed Images. Figure 3 shows the optical measurement setup to characterize the fabricated structure.

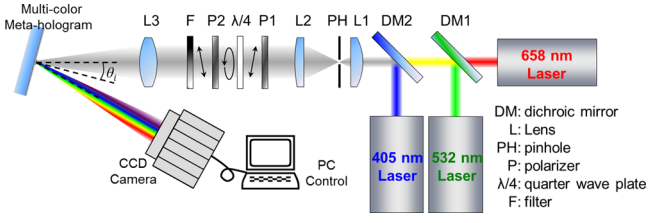

Figure 3. Measurement setup for the MCMH experiment. Using two dichroic mirrors (DM1 and DM2), three laser beams (405, 532, and 658 nm) can be combined together. Two lenses (L1 and L2) with focal lengths of 15.8 and 125 mm and one pinhole PH with a diameter of 20 μm are used as a spatial filter to modify the spot of laser beam. The polarization of the laser beam can be changed into circular polarization by the polarizer P1 and quarter-wave plate $\lambda/4$, which allows for selection of linear polarization of any angle by rotating another polarizer P2, and tuning of the intensity of laser beam is done by a filter F. The multicolor hologram is placed at the focal plane of lens L3 (focal length of 150 mm) with the incident angle $\theta_i = 12°$ which is recorded directly by a CCD camera.

We employed three laser diodes emitting at 405, 532, and 658 nm. The laser beams from the three laser diodes were combined together with two dichroic mirrors. Two lenses (focal lengths of 15.8 and 125 mm) were used to control the spot size of the combined laser beam. A spatial filter (pinhole with diameter of 20 μm) is inserted to modify the laser beam profile. Polarizer (P1) and quarter-wave plate ($\lambda/4$) are used to make the laser beam circularly polarized. Laser beam of any linear polarization angle can then be selected with equal intensity by rotating the polarizer P2. The multicolor hologram was projected onto the focal plane of lens L3 (focal length of 150 mm) with the incident angle of $\theta_i = 12°$ where the reconstructed images are recorded directly by a CCD camera.

To predict the reconstructed image of the MCMH under the illumination of three primary colors in the experiment, we used the phase and reflectance from the designed structure to simulate the images on the reconstruction plane based on fast Fourier transform. Figure 4a shows the simulated images between the −1th and 1th order in x- and y-directions. The 2-level phase hologram design has produced two images of the same letter: one at its intended position while the other upside-down at the opposite side of the zeroth-order spot located at the center of Figure 4a. The reconstructed image for any one subpixel (with period $\Lambda/2$) is the convolution between the two letters and Dirac comb function (with period $2/\Lambda$). The combination of four subpixels for the three primary colors in one pixel makes twice the period (Λ) of structure, resulting in half period of Dirac comb function and 4 times as many images. Therefore, a total of eight letter images for blue B and green G can be observed on the image plane as shown in Figure 4a.

DOI: 10.1021/acs.nanolett.5b00184
Nano Lett. 2015, 15, 3122–3127

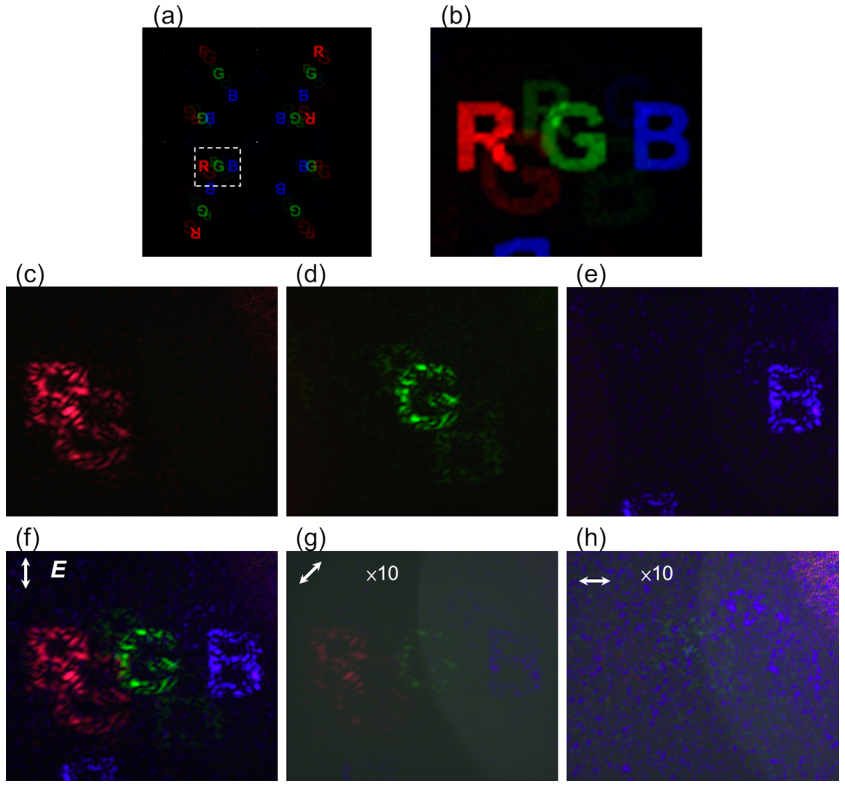

Figure 4. (a) Simulated image between the −1th and 1th order in *x*- and *y*-directions on the reconstruction plane. The dashed box indicates the recorded area by a CCD camera in measurement. (b) Magnified image from the selected region in (a) for comparison with the measurement results. The recorded images under (c) red (658 nm), (d) green (532 nm), and (e) blue (405 nm) illuminations with *y*-polarized laser beam. The images obtained by (f) *y*-polarized, (g) 45°-polarized, and (h) *x*-polarized three-color laser beam. The images obtained by linear polarized light gradually rotated from *y*-polarized (90°) to *x*-polarized (0°) are shown in the Supporting Information movie.

Note that there are total of four letter images for red R because of two (the upper left and lower right) subpixels for red in one pixel. The appearance of a letter image at a particular location depends on its wavelength with which the image is reconstructed because its diffraction angle varies with the wavelength. In Supporting Information part 3, we have shown the distance between the zeroth- and first-order images (half period on the image plane) is proportional to $\lambda/(\Lambda^2 - \lambda^2)^{1/2}$, where λ is the wavelength of incident light and Λ is the periodicity of the pixel array (Figure 2d). Using this wavelength dependence, we have designed the sizes of letters R, G, and B and their distances to the zeroth order with the normalization factor of $(\Lambda^2 - \lambda^2)^{1/2}/\lambda$ to make the reconstructed images fall into the right positions with the appearance of equal size. The function of the normalization factor is to predisperse the designed object to compensate for the chromatic dispersion of the reconstructed images. When the hologram is illuminated with a white light source obtained with the mixing of the three primary colors, each color reconstructs an image of similar size so that the chromatic blur can be easily eliminated. Figure 4b shows the enlarged region inside of the dashed box in Figure 4a. Images of the three letters of different colors and equal size are nicely positioned in a row.

The CCD recordings of reconstructed images under *y*-polarized illumination with λ = 405, 532, and 658 nm are shown in Figures 4c–e, respectively. The reconstructed image obtained with the three mixed lasers is shown in Figure 4f, exhibiting a fair agreement with the simulation result (Figure 4b). It should be pointed out that near the location of R in red there appears an unintended letter G also in red in both Figures 4c and 4f because of resonance overlap between the subpixels for letters R and G when the MCMH is illuminated in red. The efficiency is defined as the intensity ratio of the letter images to the incident light. Simulation result indicates that efficiencies for B, G, and R are 0.59%, 0.54%, and 0.69%, respectively, while that obtained from measurement for G is around 0.3%. These efficiencies are significantly lower than those of single color gold based reflective meta-holograms with multilevel-phase modulations in the near-IR[18−20] because of the much higher loss of aluminum in the visible range and the need to employ two-level phase modulation in order to reduce crosstalk to achieve color multiplexing.

Figures 4f–h show the reconstructed images collected from the MCMH sample under *y*-, 45°-, and *x*-polarized illumination exhibiting their sensitivity to light polarization. As the laser beam polarization being rotated from *y*- to *x*-direction, the recorded image gradually disappeared. (See Supporting Information movie. The angle from 90° to 0° corresponds to the polarization of incident light being rotated from *y*- to *x*-polarized.) By integrating the areas of projected letter images under *y*- and *x*-polarized incident light, we have determined the extinction ratios of 16.7 for the red R and 8.5 for both the green G and blue B. In practice, this extinction ratio is sufficient for polarization-multiplexing displays.

Aluminum Nanorod Analysis. The three primary colors demonstrated above can certainly lead to full color applications using color mixing. To further explore color tuning capabilities of aluminum nanorods employed for MCMH, we demonstrate continuous tuning of color across the visible spectrum. To this end, we fabricated six samples composed of nanorod arrays of

DOI: 10.1021/acs.nanolett.5b00184
Nano Lett. 2015, 15, 3122−3127

different aluminum rod lengths ranging from 55 to 128 nm patterned on a total area of 48 × 48 μm^2 of a 30 nm thick SiO_2 on a 130 nm thick aluminum mirror (the same unit cells we selected to realized the MCMH). Figures 5a and 5b show the

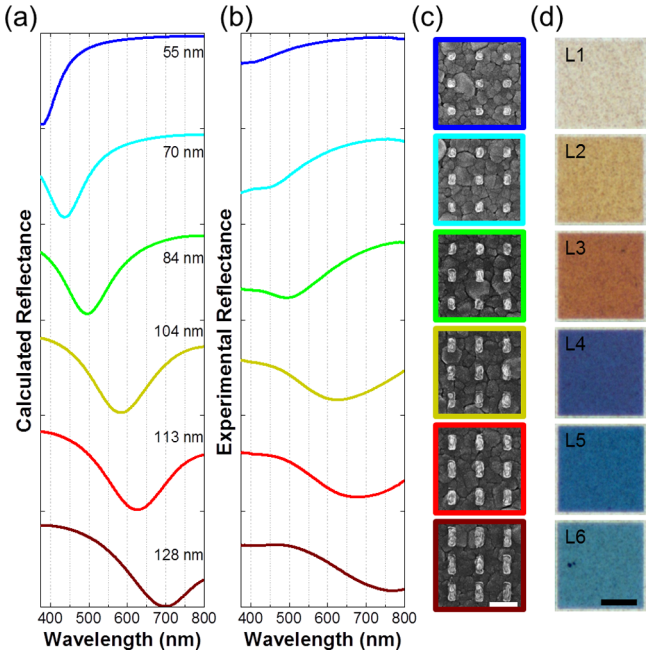

Figure 5. (a) FDTD simulation of reflectance spectra of individual nanorods with L = 55, 70, 84, 104, 113, and 128 nm. (b) Corresponding experimental reflectance spectra. (c) SEM images and (d) optical reflective images of the fabricated nanorods samples. The scale bar is 200 nm in (c) and 20 μm in (d).

simulation and measurement results of their reflectance spectra with their SEM images and optical reflective images shown in Figures 5c and 5d, respectively. The magnetic resonance continuously shifts toward longer wavelength as its rod length increases, resulting in reflective color changes from yellow through orange and blue to cyan as shown in Figure 5d corresponding to the complementary colors of each plasmonic band from blue to red. The slight differences in resonance peak position and broadening between the simulation and experiment are due to the oxidation of aluminum nanorods.[23]

Conclusion. We have demonstrated for the first time a phase-modulated full-color meta-hologram which is polarization-dependent using aluminum nanorods with resonances in red, green, and blue of the visible range. Working with the proper material combination and pixel arrays of nanorods, we have obtained narrow-bandwidth meta-hologram relative to those of prior work reported in the literatures, allowing us to implement the multicolor scheme with the three primary colors. Taking into account of the wavelength dependence of the diffraction angle, we can reconstruct images to specific locations with predetermined size. We have also demonstrated continuous color variation from blue to red with tuning of the size of aluminum nanorods that make up the pixel array. The low-cost materials of aluminum and silica make MCMH mass-producible. The polarization tunable hologram presented here can be expanded to yield dual images with the design of cross nanorods essentially composed of two sets of perpendicular aluminum rods, each used to produce one image of a particular polarization, with potential applications in performing polarization analyzer, glass-free 3D imaging, and data storage.

■ ASSOCIATED CONTENT

Supporting Information

Detailed information on reflectance and phase modulation for silver-nanorod/SiO_2/silver-mirror structure, fabrication process, and the relation between the size of a projected image vs its working wavelength. This material is available free of charge via the Internet at http://pubs.acs.org.

■ AUTHOR INFORMATION

Corresponding Author

*E-mail: dptsai@phys.ntu.edu.tw (D.P.T.).

Notes

The authors declare no competing financial interest.

■ ACKNOWLEDGMENTS

The authors acknowledge financial support from Ministry of Science and Technology, Taiwan (Grants 103-2745-M-002-004-ASP and 103-2911-I-002-594) and Academia Sinica (Grant AS-103-TP-A06). They are also grateful to National Center for Theoretical Sciences, Molecular Imaging Center of National Taiwan University, National Center for High-Performance Computing, Taiwan, and Research Center for Applied Sciences, Academia Sinica, Taiwan, for their support. G. Sun acknowledges support from AFOSR (FA9550-14-1-0196, Dr. Gernot Pomrenke, Program Manager) and AOARD (FA2386-14-1-4073, Dr. Kenneth Caster, Program Manager).

■ REFERENCES

(1) Brown, P. K.; Wald, G. *Science* **1964**, *144*, 45−51.
(2) Dowling, J. E. *The Retina: An Approachable Part of the Brain*; Harvard University Press: Cambridge, MA, 1987.
(3) Denisyuk, Y. N. *Dokl. Akad. Nauk SSSR* **1962**, *144*, 1275−1278.
(4) Haist, T.; Schonleber, M.; Tiziani, H. J. *Opt. Commun.* **1997**, *140*, 299−308.
(5) Kreis, T.; Aswendt, P.; Hofling, R. *Opt. Eng.* **2001**, *40*, 926−933.
(6) Ozaki, M.; Kato, J.; Kawata, S. *Science* **2011**, *332*, 218−220.
(7) Yu, N.; Genevet, P.; Kats, M. A.; Aieta, F.; Tetienne, J.-P.; Capasso, F.; Gaburro, Z. *Science* **2011**, *334*, 333−337.
(8) Ni, X.; Emani, N. K.; Kildishev, A. V.; Boltasseva, A.; Shalaev, V. M. *Science* **2012**, *335*, 427−427.
(9) Sun, S.; He, Q.; Xiao, S.; Xu, Q.; Li, X.; Zhou, L. *Nat. Mater.* **2012**, *11*, 426−431.
(10) Sun, S.; Yang, K.-Y.; Wang, C.-M.; Juan, T.-K.; Chen, W. T.; Liao, C. Y.; He, Q.; Xiao, S. Y.; Kung, W.-T.; Guo, G.-Y.; Zhou, L.; Tsai, D. P. *Nano Lett.* **2012**, *12*, 6223−6229.
(11) Yu, N.; Capasso, F. *Nat. Mater.* **2014**, *13*, 139−150.
(12) Larouche, S.; Tsai, Y. J.; Tyler, T.; Jokerst, N. M.; Smith, D. R. *Nat. Mater.* **2012**, *11*, 450−454.
(13) Walther, B.; Helgert, C.; Rockstuhl, C.; Setzpfandt, F.; Eilenberger, F.; Kley, E. B.; Lederer, F.; Tunnermann, A.; Pertsch, T. *Adv. Mater.* **2012**, *24*, 6300−6304.
(14) Montelongo, Y.; Tenorio-Pearl, J. O.; Milne, W. I.; Wilkinson, T. D. *Nano Lett.* **2014**, *14*, 294−298.
(15) Montelongo, Y.; Tenorio-Pearl, J. O.; Williams, C.; Zhang, S.; Milne, W. I.; Wilkinson, T. D. *Proc. Natl. Acad. Sci. U. S. A.* **2014**, *111*, 12679−12683.
(16) Ni, X. J.; Kildishev, A. V.; Shalaev, V. M. *Nat. Commun.* **2013**, *4*, 2807.
(17) Huang, L.; Chen, X.; Muhlenbernd, H.; Zhang, H.; Chen, S.; Bai, B.; Tan, Q.; Jin, G.; Cheah, K.-W.; Qiu, C.-W.; Li, J.; Zentgraf, T.; Zhang, S. *Nat. Commun.* **2013**, *4*, 2808.

DOI: 10.1021/acs.nanolett.5b00184
Nano Lett. 2015, 15, 3122−3127

(18) Chen, W. T.; Yang, K. Y.; Wang, C. M.; Huang, Y. W.; Sun, G.; Chiang, I. D.; Liao, C. Y.; Hsu, W. L.; Lin, H. T.; Sun, S.; Zhou, L.; Liu, A. Q.; Tsai, D. P. *Nano Lett.* **2014**, *14*, 225−230.
(19) Yifat, Y.; Eitan, M.; Iluz, Z.; Hanein, Y.; Boag, A.; Scheuer, J. *Nano Lett.* **2014**, *14*, 2485−2490.
(20) Zheng, G.; Mühlenbernd, H.; Kenney, M.; Li, G.; Zentgraf, T.; Zhang, S. *Nat. Nanotechnol.* **2015**, DOI: 10.1038/nnano.2015.2.
(21) Rakic, A. D.; Djurisic, A. B.; Elazar, J. M.; Majewski, M. L. *Appl. Opt.* **1998**, *37*, 5271−5283.
(22) Knight, M. W.; Liu, L. F.; Wang, Y. M.; Brown, L.; Mukherjee, S.; King, N. S.; Everitt, H. O.; Nordlander, P.; Halas, N. J. *Nano Lett.* **2012**, *12*, 6000−6004.
(23) Knight, M. W.; King, N. S.; Liu, L. F.; Everitt, H. O.; Nordlander, P.; Halas, N. J. *ACS Nano* **2014**, *8*, 834−840.
(24) Olson, J.; Manjavacas, A.; Liu, L. F.; Chang, W. S.; Foerster, B.; King, N. S.; Knight, M. W.; Nordlander, P.; Halas, N. J.; Link, S. *Proc. Natl. Acad. Sci. U. S. A.* **2014**, *111*, 14348−14353.
(25) Goh, X. M.; Zheng, Y.; Tan, S. J.; Zhang, L.; Kumar, K.; Qiu, C.-W.; Yang, J. K. W. *Nat. Commun.* **2014**, *5*, 5361.
(26) Tan, S. J.; Zhang, L.; Zhu, D.; Goh, X. M.; Wang, Y. M.; Kumar, K.; Qiu, C.-W.; Yang, J. K. W. *Nano Lett.* **2014**, *14*, 4023−4029.
(27) Shrestha, V. R.; Lee, S.; Kim, E.; Choi, D. *Nano Lett.* **2014**, *14*, 6672−6678.
(28) Zheng, B. Y.; Wang, Y.; Nordlander, P.; Halas, N. J. *Adv. Mater.* **2014**, *26*, 6318−6323.
(29) Wyrowski, F.; Bryngdahl, O. *J. Opt. Soc. Am. A* **1988**, *5*, 1058−1065.

DOI: 10.1021/acs.nanolett.5b00184
Nano Lett. 2015, 15, 3122−3127